Available online at www.sciencedirect.com
ScienceDirect
Sedimentary Geology 203 (2008) 98–111
Sedimentary Geology
www.elsevier.com/locate/sedgeo

Rutile chemistry and thermometry as provenance indicator: An example from Chios Island, Greece

Guido Meinhold [a,*], Birte Anders [a], Dimitrios Kostopoulos [b], Thomas Reischmann [c]

[a] Institut für Geowissenschaften, Johannes Gutenberg-Universität, Becherweg 21, 55099 Mainz, Germany
[b] Department of Mineralogy and Petrology, National and Kapodistrian University of Athens, Panepistimioupoli Zographou, Athens 15784, Greece
[c] Max-Planck-Institut für Chemie, Abt. Geochemie, Postfach 3060, 55020 Mainz, Germany

Received 23 May 2007; received in revised form 3 October 2007; accepted 13 November 2007

Abstract

In the present study we focused on detrital rutile separated from 12 psammitic samples that belong to three different sedimentary successions (Carboniferous, Permo-Carboniferous, Permo-Triassic) occurring on Chios Island, Greece. The Ti, Cr, Al, Fe, Nb, Zr, Si, and V contents of the rutiles were obtained by electron-microprobe analyses to trace their provenance.

The Cr and Nb concentrations of the analysed rutile grains show a wide range and indicate that this mineral in the Carboniferous succession is mainly derived from metamafic rocks, whereas in the Permo-Carboniferous and Permo-Triassic successions stem from a metapelitic source. The calculated formation temperatures using the Zr-in-rutile thermometer range from ca. 520 to 850 °C with "hotter" rutile being encountered in the Permo-Carboniferous and Permo-Triassic successions. This feature together with the rutile chemistry indicate a change in source-rock lithology through time, which could either reflect an increasing depth of erosion of an exhumed 'Variscan' nappe pile of heterogeneous composition in the hinterland or a change in the style of accretion and erosion of different terranes at the southern margin of Laurussia during the subduction of a branch of the Palaeotethys Ocean in the Late Palaeozoic. In general, this study underscores the importance of rutile chemistry and thermometry in quantitative single-mineral provenance analysis and in chemostratigraphic analysis of clastic sedimentary rocks.

Keywords: Rutile; Mineral chemistry; Sediment provenance; Aegean; Chios; Palaeotethys

1. Introduction

Knowledge of the provenance of ancient clastic sedimentary rocks is important for exploration of mineral resources, for basin analysis as well as for palaeotectonic reconstructions. Clastic sedimentary rocks are commonly composed of quartz, feldspar and mica as major constituents, and of minor amounts of heavy minerals such as zircon, rutile, tourmaline, garnet, epidote, and chrome spinel. Sediment composition is primarily affected by the composition of the initial source rock but also by a complex set of parameters such as weathering, transport, deposition and diagenesis that modify the sediment during the sedimentation cycle (e.g. Morton, 1985; Johnsson, 1993; Morton and Hallsworth, 1999). In addition to whole-rock petrography and heavy-mineral analysis, geochemical discrimination studies of whole rock and specific detrital minerals are a powerful tool in provenance characterisation, especially in deciphering tectonic processes like timing of erosion or the tectonic setting of source terrains. Most of the heavy minerals mentioned above have been used as provenance indicators for a long time by virtue of their major-, trace- and isotope-element signatures (e.g. Pober and Faupl, 1988; Morton, 1991; von Eynatten and Gaupp, 1999; Sircombe, 1999; Spiegel et al., 2002; Faupl et al., 2002), one exception being rutile (see Zack et al., 2004b) which is the focus of this study.

Here we present the results of electron-microprobe analyses and laser micro-Raman spectroscopic investigations on detrital rutiles from sedimentary rocks of Chios Island, Greece. The samples studied were taken from three different rocks units ranging in age from Late Palaeozoic to Early Mesozoic. We will discuss the application of rutile chemistry and thermometry to

* Corresponding author.
E-mail address: meinhold@uni-mainz.de (G. Meinhold).

0037-0738/$ - see front matter © 2007 Elsevier B.V. All rights reserved.
doi:10.1016/j.sedgeo.2007.11.004

single-mineral provenance analysis and compare the results obtained by using the Zr-in-rutile thermometers of Zack et al. (2004a) and Watson et al. (2006). We will furthermore evaluate the power of rutile chemistry in unravelling specific source characteristics and its use as chemostratigraphic indicator.

2. Geological setting

The island of Chios is situated in the eastern Aegean Sea (Fig. 1); tectonostratigraphically it belongs to the Hellenides, which are an integral part of the Alpine–Himalayan orogenic system in the south-eastern Mediterranean region. The Hellenides have traditionally been subdivided into Internal (hinterland) and External (foreland) zones. The Internal Hellenides comprise, from SW to NE, the Pelagonian Zone (including the Attic–Cycladic Massif), the Vardar Zone, the Serbo–Macedonian Massif and the Rhodope Massif (e.g. Jacobshagen, 1986; and references therein). All these units consist predominantly of Palaeozoic (but also Neoproterozoic and Mesozoic) basement rocks (e.g., Vavassis et al., 2000; Anders et al., 2005, 2006a,b; Turpaud and Reischmann, 2005; Himmerkus et al., 2006, in press) overlain by or intercalated with sedimentary successions. They experienced quite complex Mesozoic to Cenozoic tectonism, which gave rise to equivocal palinspastic models and interpretations.

Chios is generally assigned to the easternmost part of the Pelagonian Zone (e.g., Jacobshagen, 1986; see also discussion in Meinhold et al., 2007). It basically comprises two tectonostratigraphic units (Fig. 2): an 'autochthonous' Lower Unit and a tectonically overlying 'allochthonous' Upper Unit (Herget and Roth, 1968; Besenecker et al., 1968). A large part of the Lower Unit consists of Late Palaeozoic clastic sedimentary rocks containing blocks (of up to 100 m in diameter) of limestones, radiolarites and volcanic rocks. This succession was variably named 'Chios mélange', 'Chios (wild)flysch' or 'Volissos turbidites' (e.g., Robertson and Pickett, 2000; Groves et al., 2003; Zanchi et al., 2003). Here we use the non-genetic term Late Palaeozoic of the Lower Unit (Meinhold et al., 2007). The major rock types of this unit are greywackes, minor sandstones and siltstones as well as intercalated quartz-bearing conglomerates. The latter mainly contain clasts of quartz, black chert and quartzite, embedded in a coarse-grained quartzose matrix. Erosional contacts at the base of greywacke and conglomerate beds and upward reduction in grain size can often be observed. In some outcrops, well-developed sole marks and ripples can be seen at the base of turbidite beds. The facies of the turbidite-olistostrome succession resulted mainly from turbidity currents, debris flows and submarine slides. Groves et al. (2003) reported Mississippian microfossils from calcareous clasts of a breccia lying within the turbidite-olistostrome succession and suggested

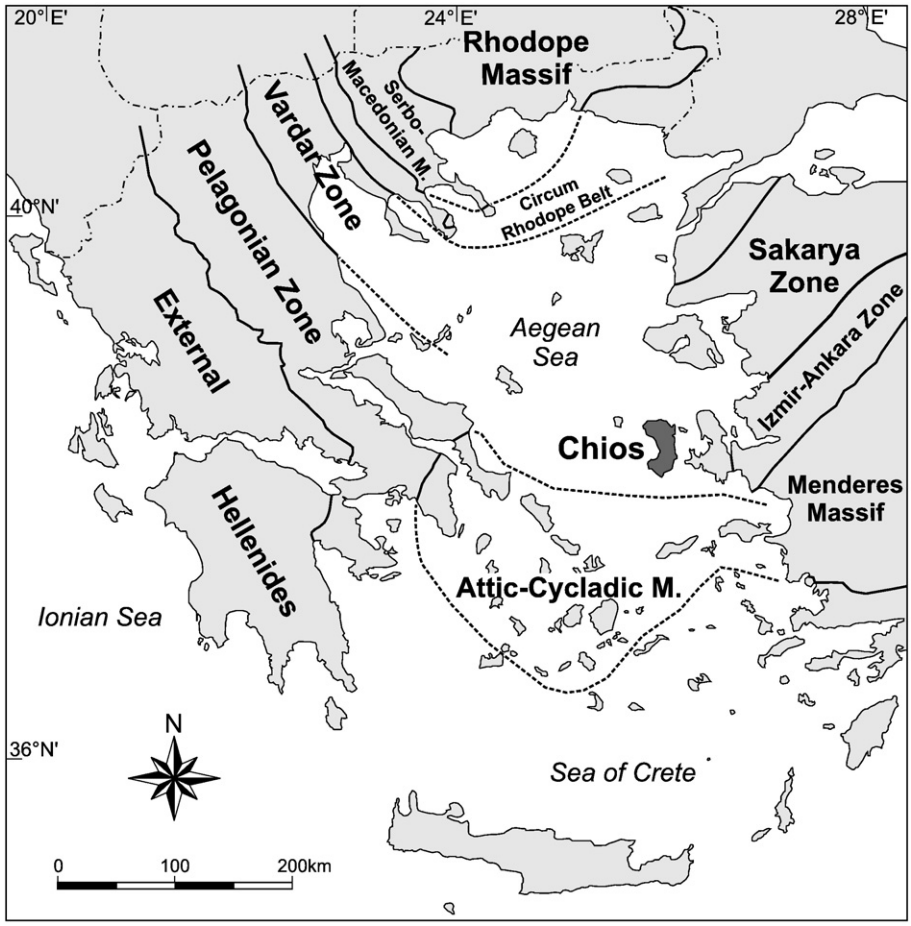

Fig. 1. Map showing the location of Chios within the Aegean region, including the main geotectonic zones (modified after Jacobshagen, 1986; Okay et al., 2001).

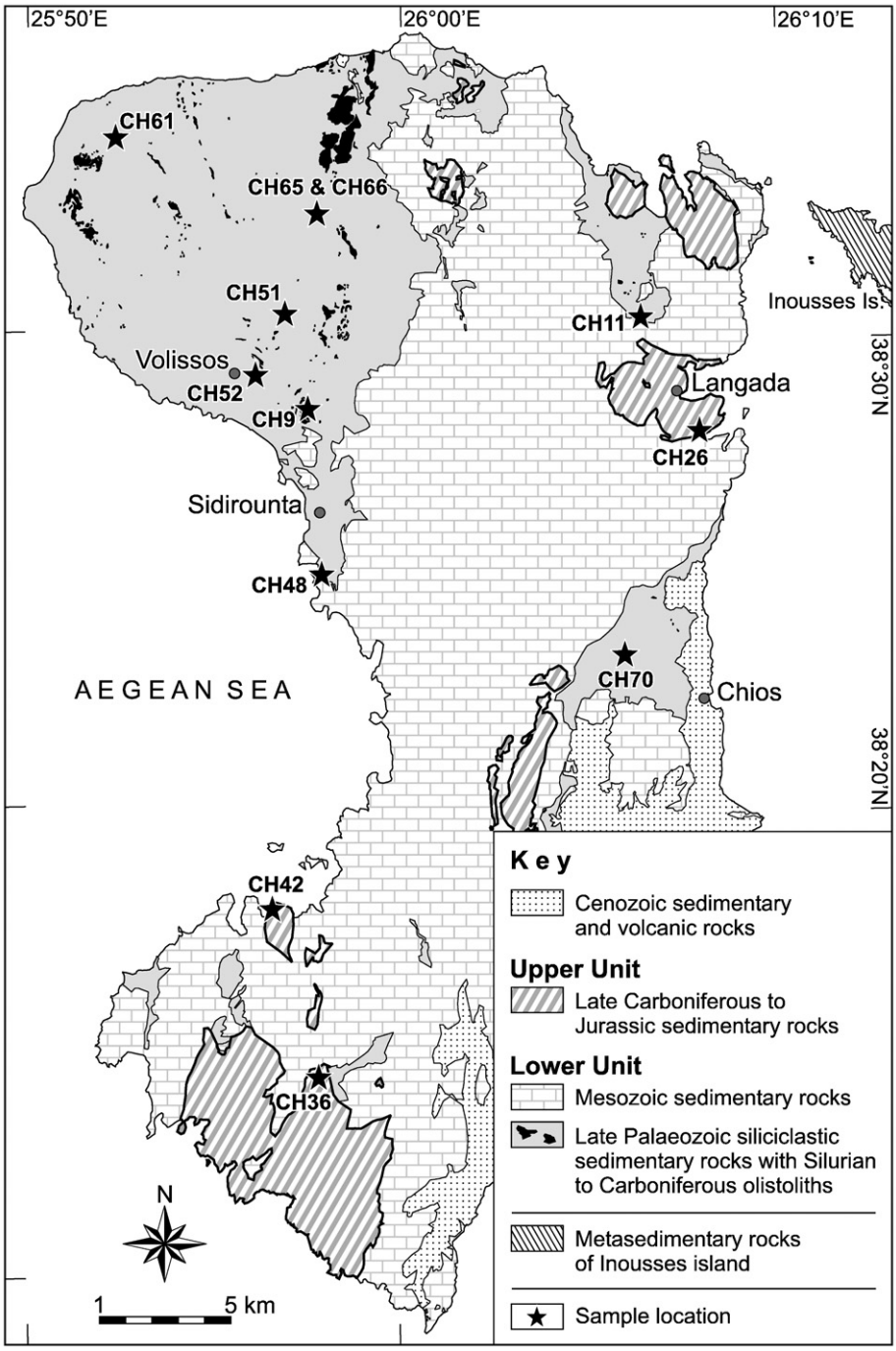

Fig. 2. Simplified geological map of Chios (after Besenecker et al., 1968, 1971). *Stars* indicate sample localities.

that the Late Palaeozoic rocks of the Lower Unit are most probably Late Visean or Early Serpukhovian in age. According to Stampfli et al. (2003) and Zanchi et al. (2003) Chios fits a geotectonic model of an arc-trench system formed along the Palaeotethyan subduction zone in Carboniferous times (cf. Robertson and Pickett, 2000; and references therein). Meinhold et al. (2007) specified a tectonic setting of a continental volcanic arc, involving upper-continental crustal rocks and/or young differentiated arc material as well as a mixed source of (ultra) mafic rocks.

The Late Palaeozoic rocks of the Lower Unit are overlain by non-fossiliferous Early Triassic conglomerates and sandstones (Besenecker et al., 1968). The conglomerates mainly contain clasts of quartz and black chert embedded in a coarse-grained quartzose matrix. Zanchi et al. (2003) described an angular unconformity at the base of this clastic succession, interpreted as a Variscan unconformity. However, the stratigraphic age of these conglomerates and sandstones is uncertain because no biostratigraphic and only few radiometric ages exist so far (Meinhold et al., 2006). The youngest detrital zircon grain

found in the Permo-Triassic sandstone so far has a rounded shape and a concordant $^{206}Pb/^{238}U$ age of ca. 326 Ma, thus giving a maximum age of deposition for this rock. Here we use the more comprehensive term Permo-Triassic instead of Early Triassic (Meinhold et al., 2007). The conglomerates and sandstones pass upwards into limestones of late Early to Late Triassic–Early Jurassic age (Besenecker et al., 1968). A Middle Triassic volcano-sedimentary succession is intercalated with the limestones (Besenecker et al., 1968; Gaetani et al., 1992). The Triassic–Jurassic transition is marked by non-marine clastic deposits followed by dolomites and limestones.

The Upper Unit of Chios belongs to the allochthonous nappe *sensu* Besenecker et al. (1968). Lithostratigraphically, its lowermost part consists of Late Carboniferous quartzose greywackes, sandstones and minor siltstones, and occasionally contains lenses of black and greenish chert a few meters in size. Layers rich in plant fossils can be found on the bedding surfaces of siltstones and fine-grained sandstones. Fossil-bearing limestones of Late Carboniferous age are overlain by an Early Permian clastic carbonaceous succession (Kauffmann, 1969). The Middle Permian is represented by fossiliferous carbonate sequences (e.g., Besenecker et al., 1968). Late Permian rocks are absent. The Permo-Carboniferous is overlain by transgressive Early Jurassic sediments which are themselves locally overlain by transgressive Upper Cretaceous deposits. The youngest rocks on Chios are Cenozoic sediments and volcanic rocks cropping out mainly in the southeastern part of the island (Fig. 2).

3. Sample description

A total of 12 psammitic samples were chosen for rutile chemical analyses. Of these, seven come from the Carboniferous and two from the Permo-Triassic part of the Lower Unit. Three Permo-Carboniferous samples were also taken from the Upper Unit of Chios. Sample locations are shown in Fig. 2; their geographic coordinates are listed in Table 1.

Table 1
Sample list

Sample	Rock type	Locality	Latitude	Longitude
Upper Unit				
Permo-Carboniferous				
CH26	greywacke	NE' Pantoukios	38°27′50.7″	26°08′01.6″
CH36	greywacke	W' Pirgi	38°14′12.1″	25°57′52.1″
CH42	greywacke	NE' Limenas	38°17′20.9″	25°56′21.1″
Lower Unit				
Permo-Triassic				
CH11	sandstone	NNW' Langada	38°30′14.2″	26°06′31.7″
CH48	sandstone	SE' Metochi bay	38°24′53.2″	25°57′52.2″
Carboniferous				
CH9	greywacke	ESE' Volissos	38°28′12.6″	25°57′33.7″
CH51	greywacke	NE' Volissos	38°30′24.5″	25°56′58.3″
CH52	greywacke	E' Volissos	38°28′58.0″	25°56′05.1″
CH61	greywacke	W' Nenitouria	38°34′05.1″	25°52′23.5″
CH65	greywacke	N' Pispilounta	38°32′28.2″	25°57′42.0″
CH66	greywacke	N' Pispilounta	38°32′28.2″	25°57′42.0″
CH70	greywacke	W' Chios	38°23′08.1″	26°06′10.1″

All samples have framework grains consisting of monocrystalline and polycrystalline quartz as well as sedimentary and volcanic lithoclasts in varying amounts. Feldspar grains are common and always present. Plagioclase (mainly albite) is by far the most abundant feldspar mineral, whereas K-feldspar is rare. Plagioclase grains often display patchy sericitisation and replacement by calcite. Single muscovite flakes and minor detrital biotite also occur. All psammites are poorly sorted by size and dominated by angular to subangular clasts. The occurrence of iron hydroxides in some samples indicates secondary alteration processes. Accessory minerals include clay minerals, opaque minerals, chlorite and heavy minerals, predominantly zircon, rutile, chrome spinel, epidote and tourmaline. The analysed sedimentary rocks are virtually non-metamorphosed or have experienced only very low-grade metamorphism, as indicated by petrology (Zanchi et al., 2003) and conodont colour alteration index data (Groves et al., 2003; Larghi et al., 2005).

The samples used here have already been investigated for their whole-rock major-, trace- and rare-earth element (REE) contents, whereas a number of them have been additionally investigated for the chemistry of detrital chrome spinel (Meinhold et al., 2007). Major- and trace-element values are compatible with a felsic to intermediate source, minor input of (ultra)mafic detritus and recycling of older sedimentary components. Chondrite-normalised REE profiles are uniform showing light REE enrichment, negative Eu anomalies and flat heavy REE patterns, indicating an upper-continental crustal source and/or young differentiated arc material. The chemistry of detrital chrome spinel suggests a mixed (ultra)mafic source involving ridge peridotites (MOR-type), fore-arc peridotites and island-arc basalts.

4. Rutile chemistry and thermometry

Rutile mainly consists of titanium dioxide (TiO_2) and is the dominant carrier (>90% of the whole-rock content) of Ti, Nb, Sb, Ta and W as well as an important carrier (5–45% of the whole-rock content) of V, Cr, Mo and Sn (Rudnick et al., 2000; Zack et al., 2002). Analyses of rutiles can nowadays be routinely performed by electron microprobe (EMP) so that differences in chemical composition can easily be identified. Rutile is mainly formed during medium- to high-grade metamorphic processes and is usually absent in igneous and low-grade metamorphic rocks (Force, 1980). Therefore, medium- to high-grade metamorphic rocks are considered to be the chief primary source of detrital rutile (Force, 1980). Additional, but minor, sources of rutile are alpine quartz veins, alkaline magmatic rocks, pegmatites, kimberlites and porphyry copper deposits (Force, 1980). Inasmuch as rutile is chemically and physically stable and not prone to destruction during the sedimentation cycle, it can provide important information about source area lithologies, and therefore, it can be used for sedimentary provenance analysis.

Few papers have been published dealing with the chemistry of detrital rutile and its application to provenance studies (e.g., Götze, 1996; Preston et al., 2002). More recently, however,

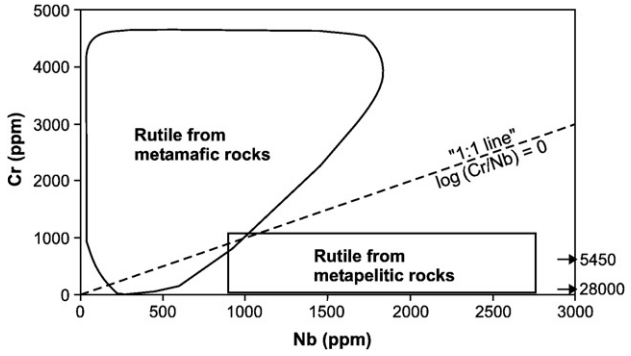

Fig. 3. Plot of Nb vs. Cr contents of rutile from different metamorphic lithologies (after Zack et al., 2004b). Arrows indicate exceptionally high Nb contents of felsic granulite-facies rocks. The "1:1 line" is taken from Triebold et al. (2005); positive log(Cr/Nb) values mostly indicate a metamafic source for rutile while negative values suggest derivation from metapelitic rocks.

rutile has attracted a lot of interest as new studies have demonstrated the high potential of the trace-element signature of rutile, including rutile thermometry, for source-rock characterisation and hence for quantitative provenance analysis (Zack et al., 2004a,b; Triebold et al., 2005, 2007; Stendal et al., 2006). The trace-element content of detrital rutile grains can discriminate between possible source rocks, for example, high-grade metamorphic rocks such as eclogites and high-pressure granulites from hydrothermal ore deposits and kimberlites (Zack et al., 2002). Moreover, Cr and Nb abundances (Fig. 3) can effectively distinguish between metamafic and metapelitic lithologies (Zack et al., 2002, 2004b), whereas the Fe content can be used as an indicator of metamorphic origin since metamorphic rutile contains mostly >1000 ppm Fe (Zack et al. 2004a). Triebold et al. (2005, 2007) introduced log(Cr/Nb) values to discriminate between metamafic and metapelitic source lithologies ("1:1" line; Fig. 3). This method is applicable, except for very low Cr and very low Nb contents. Based on literature data of Nb/TiO_2 ratios of whole rock for pelites, Zack et al. (2002, 2004b) calculated the Nb content of rutile in metapelites with 900–2700 ppm (see Fig. 3). Combined with reference data, we herein propose that the lower limit of Nb in metapelitic rutiles should be set at 800 ppm and that the discriminant boundaries between metamafic and metapelitic rocks should therefore be modified accordingly (see Fig. 4). Rutiles with negative log(Cr/Nb) values and accompanied Nb>800 ppm are interpreted to be derived from metapelitic rocks (e.g., mica-schists, paragneisses, felsic granulites) whereas positive and negative log(Cr/Nb) values, the latter however accompanied with Nb<800 ppm, suggest derivation from metamafic rocks (e.g., eclogites, mafic granulites). Rutiles from amphibolites plot in both fields because the protoliths of amphibolites are of either sedimentary or mafic igneous origin.

Zack et al. (2004a) demonstrated that the Zr concentration in rutile coexisting with quartz and zircon is strongly temperature

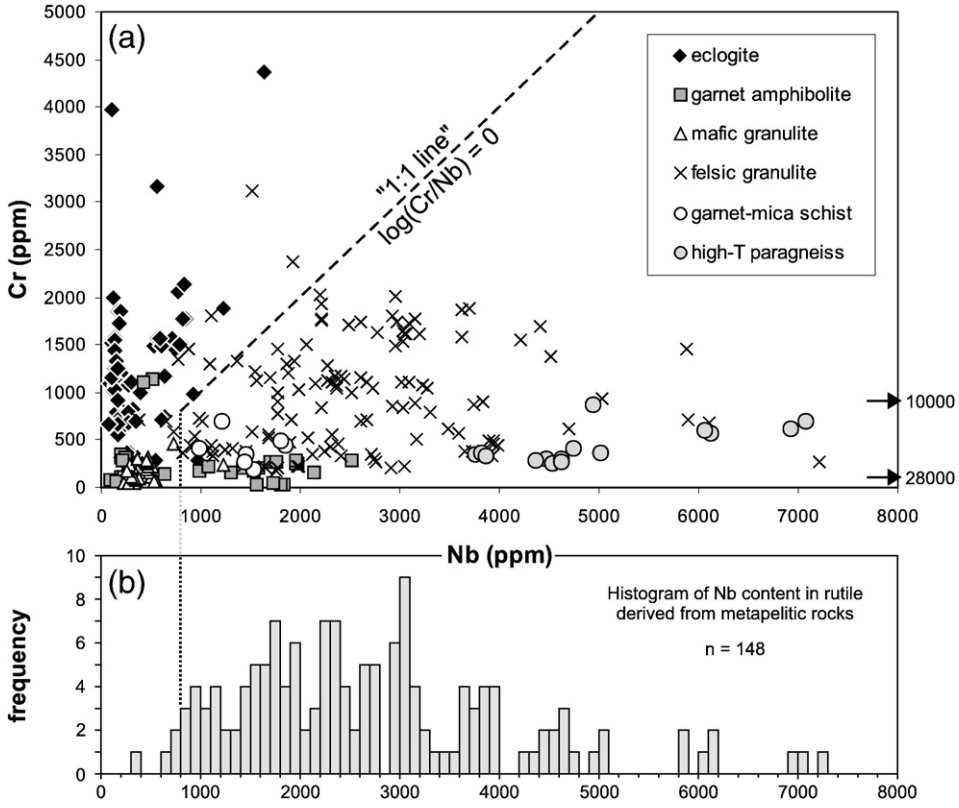

Fig. 4. (a) Plot of Nb vs. Cr contents of rutile from different metamorphic lithologies (compiled after data from Fett, 1995; Zack et al., 2002, 2004a). Arrows indicate exceptionally high Nb contents of felsic granulite-facies rocks. The "1:1 line" is according to Triebold et al. (2005). The lower limit for rutile derived from a metapelitic rock was set at 800 ppm (see Fig. 4b). (b) Histogram of Nb content in rutile derived from metapelitic rocks.

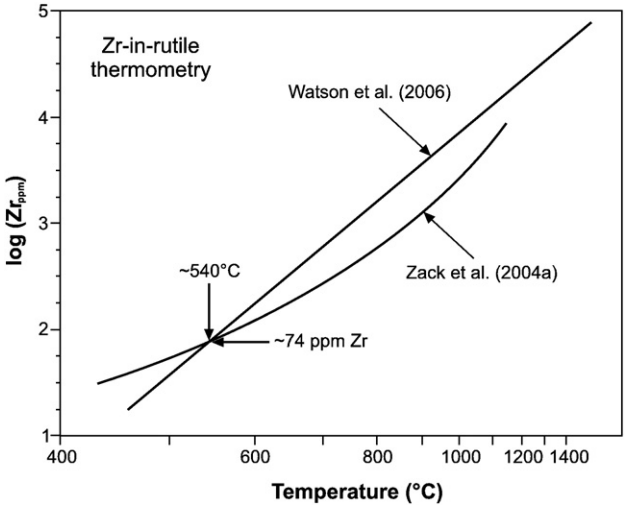

Fig. 5. Comparison of Zr-in-rutile thermometers (modified after Watson et al., 2006).

dependent. They presented an empirically calibrated Zr-in-rutile thermometer (Fig. 5), expressing temperature as:

$$T(°C) = 127.8 \times \ln(\text{Zr ppm}) - 10$$

with an error of ±50 °C. The calibration of Zack et al. (2004a) was based on analyses of rutile grains from 31 metamorphic rocks with rutile–quartz–zircon assemblages spanning a temperature range from 430 to 1100 °C. The reliability of this rutile thermometer for a wide variety of eclogites was demonstrated by Zack and Luvizotto (2006). Recently, Watson et al. (2006) presented a revised Zr-in-rutile thermometer based on experimental data and constrained by natural rutiles from metamorphic rocks (Fig. 5), expressing temperature as:

$$T(°C) = \frac{4470}{7.36 - \log_{10}(\text{Zr ppm})} - 273$$

with an error of ±20 °C. The two thermometers intersect at a temperature of ~540 °C but diverge significantly both at lower and higher temperatures (Fig. 5). Watson et al. (2006) considered this behaviour to indicate a possible pressure dependence and emphasised the need for further investigation. The successful application of the Watson et al. (2006) calibration was recently shown by Spear et al. (2006) on blueschist-facies rocks from Sifnos Island, Greece.

The combined use of detrital rutile chemistry and thermometry for quantitative provenance analysis was first applied by Zack et al. (2004b). Subsequent studies by Triebold et al. (2005, 2007) and von Eynatten et al. (2005) have demonstrated that the trace-element composition of detrital rutile is unrelated to the grain size of the host sediment and revealed that high-grade metamorphic rutile may preserve its chemical signature to much lower temperatures, meaning that rutile may survives metamorphic conditions on a retrograde path below 550 °C. Stendal et al. (2006) have also shown that relic rutile can retain its original composition during low- to medium-grade metamorphism, indicating that it can survive temperatures as high as 620 °C. Thus, the generally accepted views of rutile breakdown during low-grade metamorphic overprint (greenschist facies) and formation during medium-grade metamorphic conditions (e.g., Force, 1980; Zack et al., 2004b) may not be strictly valid.

5. Analytical methods

Rutiles were separated following standard procedures (hydraulic press, rotary mill, Wilfley table, Frantz isodynamic magnetic separator and heavy liquids [methylene iodide]). Rutile grains were hand-picked under a binocular microscope and mounted in epoxy resin, sectioned and polished. For each sample electron-microprobe analyses of randomly selected rutile grains were performed with a JEOL JXA 8900RL instrument at the University of Mainz, equipped with 5 wavelength-dispersive spectrometers. The analytical conditions of the EMP were similar to those described by Zack et al. (2004a) on a similar instrument. Each rutile grain was analysed for Ti, Cr, Al, Fe, Nb, Zr, Si and V. Operating conditions were 20 kV acceleration voltage with a beam current of 120 nA and a beam diameter of 5 μm. Detailed conditions for the spectrometers and standards used can be found in Table 2.

Areas devoid of cracks or inclusions were chosen for spot analyses. Besides single measurements (one spot per grain; Table 3) multiple analyses of selected grains were also performed to check for chemical homogeneity (Table 4). The formation temperature of each rutile grain was calculated by applying the Zr-in-rutile thermometers of both Zack et al. (2004a) and Watson et al. (2006) [abbreviated as T_Z and T_W respectively]. Since the Zr detection limit of the EMP employed is 20 ppm, the Zr-in-rutile thermometer is applicable for rutiles crystallised above ~470 °C (T_W). A complete set of mineral analyses is available as Supplementary data (see Appendix A).

In addition to EMP analyses, laser micro-Raman spectroscopy was applied to randomly selected rutile grains with variable Zr and Si contents to identify the TiO_2 structure type. Raman spectra were obtained using a Horiba Jobin Yvon HR800 spectrometer system at the University of Mainz, equipped with an Olympus BX41 optical microscope. The Raman system was operated at room temperature with an excitation wavelength of

Table 2
Conditions of the electron microprobe for rutile trace-element analyses

Spectrometer	1 TAP	2 PETJ	3 LIF	4 LIF	5 PETH
Element (Line)	Al (Kα)	Nb (Lα)	Cr (Kα)	Ti (Kβ)	Zr (Lα)
Count time	240	300	130	15	300
Bckg time	60	80	80	12	150
Standard	Al_2O_3, synthetic	Nb_2O_5, synthetic	Cr_2O_3, synthetic	TiO_2, synthetic	$ZrSiO_4$, natural
DL	15	70	20	650	20
Element (line)	Si (Kα)		Fe (Kα)	V (Kα)	
Count time	60		150	260	
Bckg time	30		75	75	
Standard	$CaSiO_3$, natural		Fe_2O_3, synthetic	V-metal, synthetic	
DL	20		20	30	

Count time counting time on the peak (in s), *Bckg time* counting time on background position (in s), *DL* detection limit (in ppm).

Table 3
Summary of detrital rutile analyses; single measurements (one spot per grain)

Unit	Lower Unit									Upper Unit		
Stratigraphy	Carboniferous							Permo-Triassic		Permo-Carboniferous		
Sample	CH9	CH51	CH52	CH61	CH65	CH66	CH70	CH11	CH48	CH26	CH36	CH42
Grains	15	20	33	20	41	19	32	49	40	57	55	20
Cr (ppm)												
Minimum	281	68	b.d.	b.d.	b.d.	185	68	b.d.	b.d.	96	b.d.	82
Maximum	6603	4201	2080	1409	2737	2326	8703	6972	4885	4632	2703	2135
Average	1490	1024	985	686	819	940	1104	1168	1080	1123	928	641
SD	1803	990	471	431	672	563	1553	1538	1170	971	582	516
Al (ppm)												
Minimum	53	53	58	53	53	53	53	53	53	53	53	53
Maximum	228	1784	566	381	693	164	513	1249	333	688	582	752
Average	118	207	132	124	161	97	173	166	104	108	199	129
SD	69	388	94	75	125	38	131	252	60	92	145	157
Fe (ppm)												
Minimum	257	567	606	645	645	326	194	225	326	218	295	762
Maximum	5853	5037	4190	3513	3537	2107	4998	5371	4462	5029	3879	3615
Average	3114	2276	1806	1536	1830	1404	1907	1745	1885	1641	1964	1874
SD	1739	1120	790	730	694	515	1061	1191	1140	1212	858	858
Nb (ppm)												
Minimum	308	84	b.d.	b.d.	70	b.d.	126	147	70	112	98	364
Maximum	3034	8081	3915	3286	3586	2461	5432	8794	6222	5767	5956	4600
Average	1541	1773	742	852	858	626	1540	2038	2041	1861	2045	1751
SD	1104	2152	731	969	774	632	1550	1772	1618	1250	1513	1124
Zr (ppm)												
Minimum	b.d.	96	104	81	74	89	74	b.d.	52	59	52	89
Maximum	2561	703	1118	763	800	1022	1229	2391	5256	3220	629	1866
Average	301	324	369	322	317	395	331	494	585	787	247	386
SD	680	179	255	187	174	275	246	437	832	719	111	403
Si (ppm)												
Minimum	79	93	79	98	89	93	79	75	93	70	70	75
Maximum	192	229	215	425	1159	201	430	1744	351	916	290	276
Average	108	135	127	143	136	116	123	142	139	109	95	95
SD	30	29	31	73	164	26	59	246	56	113	38	47
V (ppm)												
Minimum	b.d.	421	421	231	204	360	306	b.d.	170	190	b.d.	170
Maximum	2243	2875	2536	2318	3045	4208	2739	6036	3168	5615	4847	3508
Average	591	1226	1212	879	1352	1738	1163	2171	1435	1984	1514	1155
SD	551	597	602	576	666	941	462	1207	750	1046	803	799
T_W (°C)												
Minimum	541	558	563	547	541	553	541	527	519	527	519	553
Maximum	858	718	764	725	730	754	774	850	955	887	707	820
Average	589	638	645	638	637	650	637	663	666	695	620	641
SD	84	48	55	46	45	58	52	69	85	92	37	65
T_Z (°C)												
Minimum	540	574	583	552	540	563	540	512	495	512	495	563
Maximum	993	828	887	838	844	876	899	984	1085	1022	814	953
Average	619	708	718	709	707	726	705	743	743	785	681	711
SD	119	77	86	73	72	90	81	103	124	134	63	96

One grain from sample CH9 that was identified as anatase by laser micro-Raman spectroscopy was excluded from measurement statistics. See text for explanation.

632.8 nm. Titanium dioxide occurs in nature in three structural states. The most common is rutile (tetragonal) which is the high-temperature polymorph. The low-temperature polymorphs are anatase (tetragonal) and brookite (orthorhombic). Rutile was identified by Raman bands at 143, 247, 447, and 612 cm^{-1} (Porto et al., 1967; Tompsett et al., 1995) and anatase by bands at

Table 4
Summary of detrital rutile analyses; multiple measurements (several spots per grain)

Unit	Lower Unit											Upper Unit				
Stratigraphy	Carboniferous						Permo-Triassic					Permo-Carboniferous				
Sample	CH52	CH65	CH66	CH70	CH70	CH70	CH11	CH11	CH48	CH48	CH48	CH26	CH26	CH26	CH26	CH42
Grain no.	31	5	10	1	5	19	12	51	11	12	34	1	4	15	17	2
Spots	10	11	4	11	42	3	4	39	3	4	3	3	3	4	3	4
Cr (ppm)																
Minimum	807	999	869	246	520	8518	1375	4933	109	2251	1498	1758	2833	185	151	2135
Maximum	848	1492	931	335	657	8888	1451	6842	144	2340	1539	1765	2915	219	164	2183
Average	827	1128	893	286	604	8703	1423	6202	130	2299	1524	1763	2885	197	157	2157
SD	14	141	30	24	33	185	34	564	18	37	22	4	46	16	7	23
Al (ppm)																
Minimum	180	58	101	296	53	53	53	53	79	58	180	138	74	122	53	58
Maximum	259	122	164	1154	164	58	572	1530	90	111	228	243	79	143	53	69
Average	216	80	132	540	76	55	255	118	85	83	208	178	76	136	53	64
SD	23	20	26	225	20	3	252	249	5	26	25	57	3	10	0	4
Fe (ppm)																
Minimum	2192	1508	1866	2301	591	194	225	521	1710	257	505	303	738	933	3218	1275
Maximum	3109	1873	2029	3140	1158	241	1003	1011	1866	1182	637	567	793	1026	4174	1609
Average	2621	1740	1972	2619	878	210	519	650	1780	573	567	420	767	987	3798	1469
SD	336	94	74	232	125	27	342	110	79	415	66	135	27	41	510	150
Nb (ppm)																
Minimum	615	601	1314	1964	70	419	790	559	2684	1720	2405	1755	1000	280	4187	1035
Maximum	783	1111	1699	2174	182	440	930	1307	2852	1762	2531	2307	1132	377	5697	1160
Average	710	812	1520	2072	119	426	842	878	2766	1739	2486	2083	1084	325	4935	1094
SD	51	173	184	62	31	12	63	195	84	19	71	291	73	49	755	52
Zr (ppm)																
Minimum	437	222	999	141	267	1222	2280	111	5241	1096	940	1621	2265	1762	688	1836
Maximum	503	348	1022	185	437	1236	2421	222	5256	1259	1125	1777	2339	2014	777	1917
Average	471	290	1012	165	348	1229	2347	178	5246	1170	1027	1698	2307	1892	745	1879
SD	23	41	9	17	41	7	70	25	9	83	93	78	38	126	49	35
Si (ppm)																
Minimum	79	89	89	89	56	98	75	79	89	79	103	117	65	75	75	75
Maximum	122	122	122	257	346	112	827	2323	122	164	187	215	75	89	75	131
Average	95	105	104	115	113	108	370	199	108	116	132	160	72	82	75	93
SD	14	11	15	48	58	8	348	368	17	35	47	50	5	6	0	25
V (ppm)																
Minimum	2447	1394	863	1258	836	1597	4371	3236	1516	2338	890	2705	2284	1332	1176	1795
Maximum	2556	1747	897	1339	1006	1686	4480	4235	1625	2393	938	2787	2536	1394	1502	2121
Average	2504	1621	879	1301	921	1631	4437	3849	1552	2367	913	2739	2440	1370	1312	1965
SD	36	89	15	24	42	48	49	314	63	30	24	42	136	27	170	138
T_W (°C)																
Minimum	674	619	752	585	633	773	844	568	955	762	746	804	843	814	715	818
Maximum	687	655	754	605	674	774	851	619	955	776	764	814	847	829	727	823
Average	681	639	753	596	654	774	847	601	955	768	755	809	845	822	723	821
SD	4	12	1	8	10	1	4	11	0	7	9	5	2	8	6	2
T_Z (°C)																
Minimum	767	681	873	622	704	898	978	592	1085	884	865	935	977	945	825	950
Maximum	785	738	876	657	767	900	986	681	1085	902	888	946	981	962	841	956
Average	776	713	874	642	737	899	982	651	1085	893	876	940	980	954	835	953
SD	6	19	1	13	15	1	4	19	0	9	12	6	2	9	9	2

See text for explanation.

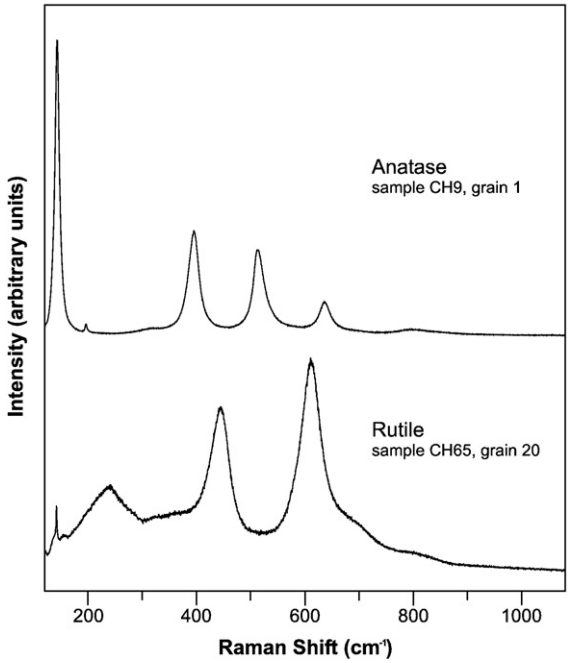

Fig. 6. Laser Raman spectrum of rutile from sample CH65 (grain no. 20) compared with the spectrum of anatase from sample CH9 (grain no. 1).

144, 197, 400, 516, and 640 cm^{-1} (Ohsaka et al., 1978). Brookite is characterised by several bands; strong ones are at 153, 247, 322, and 636 cm^{-1} (Tompsett et al., 1995). The grains analysed by laser micro-Raman spectroscopy are indicated in the Supplementary data.

6. Results

The analysed rutiles from Chios vary in size from a few µm to 0.4 mm and are yellowish to reddish-brown in colour. The results of 399 single and 151 multiple (16 grains) EMP spot measurements are summarised in Tables 3 and 4 respectively.

There is a large variation in the trace-element composition of rutile in all samples analysed: Cr: <20–8703 ppm, Al: 53–1784 ppm, Fe: 194–5853 ppm, Nb: <70–8794 ppm, Zr: <20–5256 ppm, Si: 70–1744 ppm and V: <30–6036 ppm. Those grains with abnormally low or high Zr and Si contents (23 in all) were additionally analysed by laser micro-Raman spectroscopy. All Raman spectra are characteristic of rutile with the exception of one grain which is clearly anatase (Fig. 6). Brookite was not found in the analysed samples. The EMP analysis of the anatase grain is also included in the Supplementary data; this grain, however, was not considered any further in provenance analysis.

The chemical variability of rutile was tested by multiple measurements on single grains. An example is shown in Fig. 7. Eleven spot measurements on grain 1 from sample CH70 demonstrate that the chemical variability of the Zr content (141–185 ppm) is within the range of the error of the applied Zr-in-rutile thermometer. The variability of the contents in Cr (246–335 ppm) and Nb (1964–2174 ppm) is negligible relative to the overall variability considered here (see Fig. 8), taking into

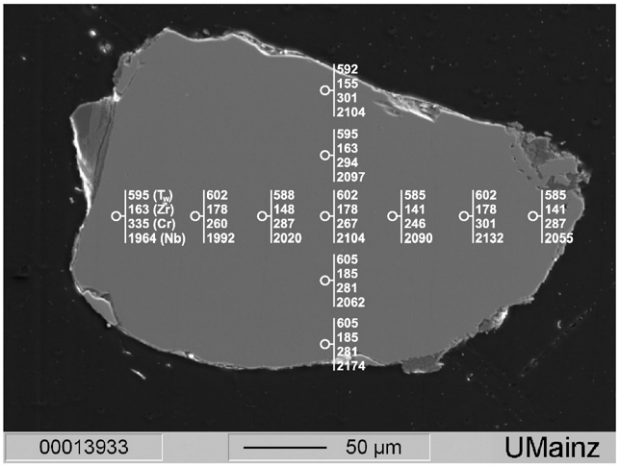

Fig. 7. Secondary electron image of rutile from sample CH70 (grain no. 1) used for multiple measurements. Circles mark the location of the spots analysed. The numbers give T_W in °C and the concentrations of Zr, Cr and Nb in ppm for the indicated spots. Calculated temperatures range between 585 and 605 °C indicating a homogenous distribution of Zr-in-rutile (see text for discussion).

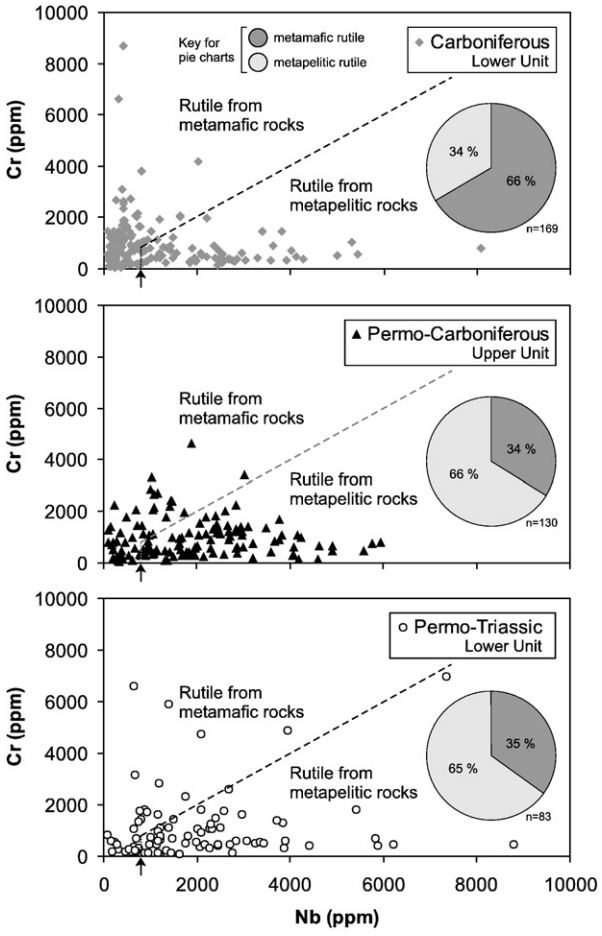

Fig. 8. Plot of Nb vs. Cr contents of detrital rutiles. The fields for rutile derived from metamafic and metapelitic rocks are according to Triebold et al. (2005) whereas the lower limit for rutile derived from a metapelitic source rock is set at 800 ppm, marked by an arrow. The discrimination between metamafic and metapelitic rutiles is additionally shown in pie charts (insets).

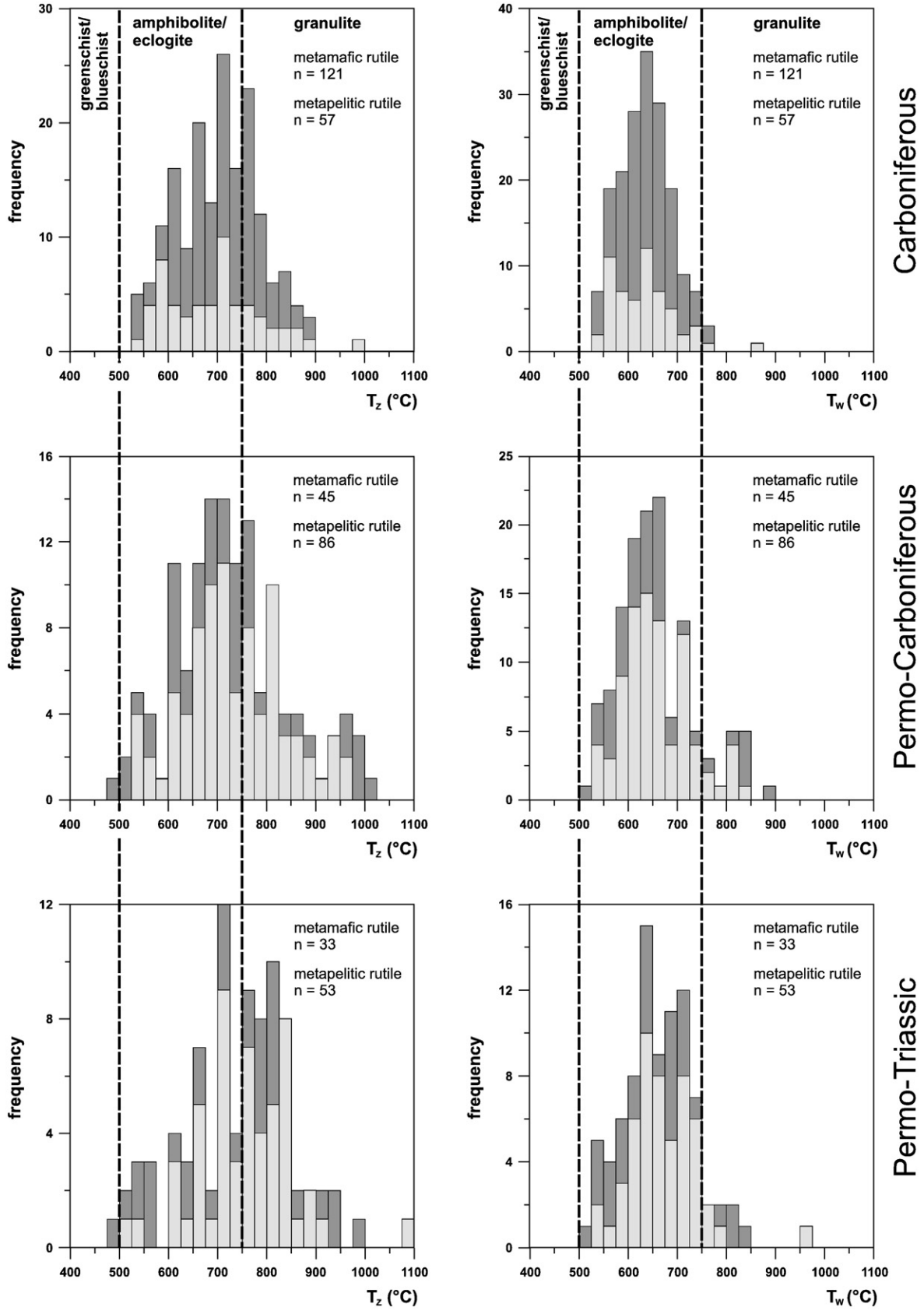

Fig. 9. Histograms of calculated formation temperatures for metamafic and metapelitic rutiles analysed from each unit. On the *left side* the equation of Zack et al. (2004a) was used, on the *right side* the equation of Watson et al. (2006) was applied. Approximate temperature boundaries of metamorphic facies for metapelitic rutile are shown for comparison following Zack et al. (2004b).

account the analytical error. The Zr-in-rutile thermometer (T_W formalism) yielded temperatures within a narrow range (585–605 °C). Combined with the data in Table 4 , it suggests that for our case study one spot measurement per grain is enough for quantitative single-mineral provenance analysis to distinguish different rutile generations according to their formation temperature.

According to the Nb vs. Cr diagram and pie charts (Fig. 8) our data indicate a mixed rutile source for all three Chios successions, with a more pronounced metamafic source in Carboniferous times (especially for the Lower Unit) and a more pronounced metapelitic source in Permo-Triassic times. The low Fe contents (<1000 ppm) of the few Cr-rich rutiles (Cr>3000 ppm) probably hint at their magmatic origin since metamorphic rutile generally contains >1000 ppm Fe (Zack et al., 2004a).

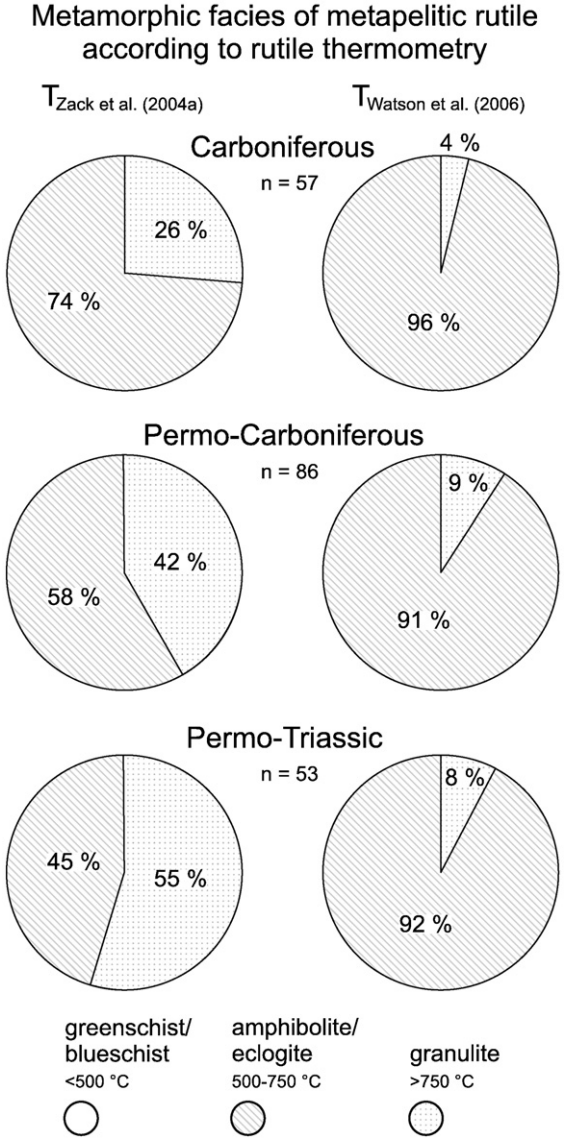

Fig. 10. Pie charts showing the percentage of different metamorphic facies for the source rocks of metapelitic rutile according to calculated formation temperatures in Fig. 9.

The results of Zr-in-rutile thermometry are shown as histograms in Figs. 9 (all rutiles) and 10 (metapelitic rutiles only). Here it is noteworthy that the application of Zr-in-rutile thermometry to detrital rutile is based on the assumption that the source rocks for the rutile had a stable rutile–quartz–zircon assemblage (Zack et al., 2004a,b). Because quartz and zircon are characteristically common in metapelitic rocks, Zr-in-rutile thermometry is applicable for those rocks (Zack et al., 2004a,b). The presence of rutile coexisting with quartz and zircon, however, is not always given in a mafic rock that seems to restrict the application of Zr-in-rutile thermometry. But meanwhile there is some evidence that the Zr-in-rutile thermometer may also work with more mafic lithologies (H. von Eynatten, pers. comm., 2007).

In this case study, calculated temperatures range between ca. 495–1000 °C (T_Z formalism) and ca. 520–850 °C (T_W formalism) respectively (Fig. 9). In general, the thermometer of Zack et al. (2004a) gives a wider spread and higher formation temperatures for the same rutile grain than the thermometer of Watson et al. (2006), except for grains with <74 ppm Zr (see Fig. 5). Nevertheless, both thermometers show a shift towards "hotter" rutiles in both the Permo-Carboniferous and the Permo-Triassic samples. High Zr concentrations in our rutiles are not accompanied by high Si values; we therefore interpret the high temperatures calculated for these grains as real formation temperatures and not due to submicroscopic zircon inclusions. It is interesting to note that the highest Zr contents (>1000 ppm) and, by implication, the highest calculated formation temperatures (e.g., T_W>750 °C) are restricted to rutiles with Nb<2500 ppm and Cr<3500 ppm. Moreover, the highest calculated temperatures belong to metapelitic rutiles.

As Fig. 9 indicates there is no input of metapelitic rutile from greenschist- or blueschist-facies rocks, instead, amphibolite- and eclogite-facies lithologies are the most plausible candidates for this type of rutile, whereas the contribution of granulite-facies rocks depends critically on the thermometer adopted. Granulite-facies sources become important only in the Permo-Carboniferous and Permo-Triassic samples, as can be clearly seen from Fig. 10. However, the T_Z formalism requires that about 50% of the rutiles from the Permo-Carboniferous and Permo-Triassic samples be derived from granulite-facies sources for which we find no solid geological evidence so far. For this reason we will adhere, in this paper, to the thermometer of Watson et al. (2006). It is nonetheless significant that even using the latter thermometer at least ca. 8% of the detrital rutile in Permo-Carboniferous and Permo-Triassic times seems to have originated from high-grade metamorphic gneiss terranes.

7. Discussion and conclusions

The chemistry and thermometry of detrital rutile from clastic sedimentary rocks of Chios have provided important information about the lithology of their source rocks and allow a chemostratigraphic distinction to be made between the Carboniferous samples on the one hand and the Permo-Carboniferous and Permo-Triassic samples on the other. Rutile Cr–Nb systematic indicates a major input from metamafic lithologies in

the Carboniferous succession and a major input from metapelitic lithologies in the Permo-Carboniferous and Permo-Triassic successions. The presence of detrital chrome spinel in the clastic sedimentary successions of Chios confirms an input from (ultra) mafic rocks (e.g., Meinhold et al., 2007). The calculated rutile formation temperatures (T_W formalism) range between ca. 520 and 850 °C with "hotter" rutile being encountered in the Permo-Carboniferous and Permo-Triassic successions. The source of rutiles derived from amphibolite- and eclogite-facies rocks could be sought in basement rocks of Pelagonia (which comprises the Pelagonian Zone and the Attic–Cycladic Massif), Sakarya, the Balkan region and the Menderes Massif since amphibolite- and eclogite-facies rocks of pre-Triassic age have been reported there (e.g., Candan et al., 2001; Mposkos et al., 2001; Anders et al., 2006b; Carrigan et al., 2006; Okay et al., 2006; and references therein). Another potential source for the detrital rutiles of Chios could be pre-Triassic syenites, diorites, pegmatites and quartz veins. The latter two, although volumetrically minor, show a wide range in chemical composition (e.g., Uher et al., 1998; Rudnick et al., 2000; Zack et al., 2002; Okrusch et al., 2003). The source of rutile derived from high-grade metamorphic gneiss terranes ($T>750$ °C) cannot yet be identified with confidence. To our knowledge, there are only few localities in the neighbouring Aegean region where granulite-facies rocks of pre-Triassic age have been recognised. The closest locality to Chios is the core series of the Menderes Massif in western Turkey (e.g., Candan et al., 2001; and references therein) where late Pan-African (583.0±5.7 Ma) pelitic granulites have been dated (Koralay et al., 2006). A sediment supply from the Menderes Massif into the clastic sediments of Chios in Late Palaeozoic and Early Triassic times would have an impact on palinspastic reconstructions of the eastern Mediterranean. However, such an in-depth analysis is beyond the scope of the present paper. High-grade metamorphic gneisses have also been documented from the Balkan region. Carrigan et al. (2006) reported Early Carboniferous (Viséan) high-grade metamorphism from the Sredna Gora Zone of Bulgaria. Pre-Alpine (latest Carboniferous) high-T low-P metamorphism with maximum temperatures exceeding 640 °C was reported for high-alumina metapelitic rocks from the Vernon Massif in the Pelagonian Zone (Mposkos et al., 2001). Furthermore, Early Carboniferous (Viséan–Serpukhovian) high-T medium-P metamorphism and anatexis have been documented for gneisses and pegmatites of the Pulur Massif in the Eastern Pontides (Topuz et al., 2004). If we consider fast exhumation of such 'Variscan' units to the surface and erosion in Permo-Carboniferous times, high-grade metamorphic rocks similar to those exposed nowadays in the Balkan region, in parts of Pelagonia and Sakarya as well as in the Pontides could well have been a source of granulite-facies rutile. Another explanation for the source of granulite-facies rutiles might be recycling of older rutile grains (see Zack et al., 2004b). Geochronological studies indicate an input of Grenvillian (ca. 1 Ga) and Eburnean (ca. 2 Ga) zircons into the Permo-Triassic succession of Chios for which a heterogeneous northern Gondwana-derived source was proposed (Meinhold et al., 2006). Because zircon and rutile behave similarly during the sedimentation cycle, it seems reasonable to assume a minor input of Grenvillian and Eburnean rutile as well.

In general, rutile chemistry in combination with rutile thermometry indicate a change in source-rock lithology through time, with more metamafic rocks of low to medium-grade eroding in Carboniferous times and more metapelitic rocks of medium to high-grade eroding in Late Carboniferous to Early Triassic times. However, the question arises as to what caused this shift in source composition from the Carboniferous to the Early Triassic. Present palaeotectonic models (e.g., Stampfli et al., 2003) suggest a fore-arc basin setting for the Chios successions in Carboniferous times with northward subduction of the Palaeotethys Ocean beneath the southern margin of Laurussia that switched to a back-arc setting during the Permian and Triassic. This switch in setting probably caused a change in source lithology attested to by a concomitant change in rutile chemistry. It could reflect either an increasing erosion depth of an exhumed 'Variscan' nappe pile of heterogeneous composition in the hinterland (collapsing 'Variscan cordillera': Stampfli et al., 2003, Fig. 8) or a change in the style of accretion and erosion of different terranes, probably accompanied by large-scale transcurrent movements (e.g. Stampfli et al., 2002, Fig. 4), placing very different oceanic or continental fragments next to each other during the subduction of a branch of the Palaeotethys Ocean in the Late Palaeozoic.

Acknowledgements

We want to thank Nora Groschopf, Burkhard Schulz-Dobrick and Tobias Häger for technical assistance. Laboratory facilities at the Max Planck Institute for Chemistry in Mainz are kindly appreciated. Financial support is acknowledged from the German Research Foundation (DFG) and the state of Rhineland-Palatinate through the Graduiertenkolleg 392 "Composition and Evolution of Crust and Mantle". Heinrich Bahlburg and Hilmar von Eynatten are thanked for thorough reviews.

Appendix A. Supplementary data

Supplementary data associated with this article can be found, in the online version, at doi:10.1016/j.sedgeo.2007.11.004.

References

Anders, B., Reischmann, T., Poller, U., Kostopoulos, D., 2005. Age and origin of granitic rocks of the eastern Vardar Zone, Greece: new constraints on the evolution of the Internal Hellenides. J. Geol. Soc. Lond. 162, 857–870.

Anders, B., Reischmann, T., Kostopoulos, D., 2006a. Zircon geochronology of basement rocks from the Pelagonian Zone, Greece: constraints on the pre-Alpine evolution of the westernmost Internal Hellenides. Int. J. Earth Sci. doi:10.1007/s00531-006-0121-7.

Anders, B., Reischmann, T., Kostopoulos, D., Poller, U., 2006b. The oldest rocks of Greece: first evidence for a Precambrian terrane within the Pelagonian Zone. Geol. Mag. 143, 41–58.

Besenecker, H., Dürr, S., Herget, G., Jacobshagen, V., Kauffmann, G., Lüdtke, G., Roth, W., Tietze, K.W., 1968. Geologie von Chios (Ägäis). Geol. et Palaeont. 2, 121–150.

Besenecker, H., Dürr, S., Herget, G., Kauffmann, G., Lüdtke, G., Roth, W., Tietze, K.W., 1971. Geological Map of Greece, Chios sheet, 1 : 50 000 (2 sheets: Northern and Southern). Inst. Geol. Subsurface Res., Athens.

Candan, O., Dora, O., Oberhänsli, R., Çetinkaplan, M., Partzsch, J., Warkus, F., Dürr, S., 2001. Pan-African high-pressure metamorphism in the Precambrian basement of the Menderes Massif, western Anatolia, Turkey. Int. J. Earth Sci. 89, 793–811.

Carrigan, C.W., Mukasa, S.B., Haydoutov, I., Kolcheva, K., 2006. Neoproterozoic magmatism and Carboniferous high-grade metamorphism in the Sredna Gora Zone, Bulgaria: an extension of the Gondwana-derived Avalonian–Cadomian belt? Precambrian Res. 147, 404–416.

Faupl, P., Petrakakis, K., Migiros, G., Pavlopoulos, A., 2002. Detrital blue amphiboles from the western Othrys Mountain and their relationship to the blueschist terrains of the Hellenides (Greece). Int. J. Earth Sci. 91, 433–444.

Fett, A., 1995. Elementverteilung zwischen Granat, Klinopyroxen und Rutil in Eklogiten-Experiment und Natur. PhD dissertation. University of Mainz, 227 pp.

Force, E.R., 1980. The provenance of rutile. J. Sediment. Petrol. 50, 485–488.

Gaetani, M., Jacobshagen, V., Nicora, A., Kauffmann, G., Tselepides, V., Fantini Sestini, N., Mertmann, D., Skourtsis-Coroneou, V., 1992. The Early–Middle Triassic boundary at Chios (Greece). Riv. Ital. Paleont. Strat. 98, 181–204.

Götze, J., 1996. Genetic information of accessory minerals in clastic sediments. Zentralbl. Geol. Paläontol., Teil 1 1995, 101–118.

Groves, J.R., Larghi, C., Nicora, A., Rettori, R., 2003. Mississippian (Lower Carboniferous) microfossils from the Chios Melange (Chios Island, Greece). Geobios 36, 379–389.

Herget, G., Roth, W., 1968. Stratigraphie des Paläozoikums im Nordwest-Teil der Insel Chios (Ägäis). N. Jb. Geol. Paläont. Abh. 131, 46–71.

Himmerkus, F., Reischmann, T., Kostopoulos, D., 2006. Late Proterozoic and Silurian basement units within the Serbo–Macedonian Massif, northern Greece: the significance of terrane accretion in the Hellenides. In: Robertson, A.H.F., Mountrakis, D. (Eds.), Tectonic Development of the Eastern Mediterranean Region. Geol. Soc. Lond., Spec. Publ., vol. 260, pp. 35–50.

Himmerkus, F., Anders, B., Reischmann, T., Kostopoulos, D., in press. Gondwana-derived terranes in the northern Hellenides. In: Hatcher Jr., R.D., Carlson, M.P., McBride, J.H., Martínez Catalán, J.R. (Eds.), 4-D Framework of Continental Crust. Geol. Soc. Am., Mem., vol. 200.

Jacobshagen, V., 1986. Geologie von Griechenland. Beitr. Reg. Geol. Erde 19, 363 pp.

Johnsson, M.J., 1993. The system controlling the composition of clastic sediments. In: Johnsson, M.J., Basu, A. (Eds.), Processes Controlling the Composition of Clastic Sediments. Geol. Soc. Am., Spec. Pap., vol. 284, pp. 1–19.

Kauffmann, G., 1969. Die Geologie von Nordost-Chios (Ägäis). PhD dissertation, University of Marburg, 212 pp.

Koralay, O.E., Chen, F., Oberhänsli, R., Wan, Y., Candan, O., 2006. Age of granulite facies metamorphism in the Menderes Massif, Western Anatolia / Turkey: Shrimp U–Pb zircon dating. Abstr. 59th Geol. Congress Turkey, 20–24 March 2006, Ankara.

Larghi, C., Cordey, F., Corradini, C., Gaetani, M., Nicora, A., 2005. Palaeozoic (Silurian and Devonian) radiolarians and conodonts from chert olistoliths of the Volissos Turbidites, Chios island, Greece. Eclogae geol. Helv. 98, 123–131.

Meinhold, G., Kostopoulos, D., Reischmann, T., 2007. Geochemical constraints on the provenance and depositional setting of sedimentary rocks from the islands of Chios, Inousses and Psara, Aegean Sea, Greece: implications for the evolution of Palaeotethys. J. Geol. Soc. Lond. 164, 1145–1163.

Meinhold, G., Kostopoulos, D., Reischmann, T., Matukov, D., Sergeev, S., 2006. Provenance of Permo-Triassic clastic sediments from Chios Island, Greece, using detrital zircon ages. Geophys. Res. Abstr. 8, 04496.

Morton, A.C., 1985. Heavy minerals in provenance studies. In: Zuffa, G.G. (Ed.), Provenance of Arenites. Reidel, Dordrecht, pp. 249–277.

Morton, A.C., 1991. Geochemical studies of detrital heavy minerals and their application to provenance research. In: Morton, A.C., Todd, S.P., Haughton, P.D.W. (Eds.), Developments in Sedimentary Provenance Studies. Geol. Soc. London, Spec. Publ., vol. 57, pp. 31–45.

Morton, A.C., Hallsworth, C.R., 1999. Processes controlling the composition of detrital heavy mineral assemblages in sandstones. Sediment. Geol. 124, 3–29.

Mposkos, E., Kostopoulos, D.K., Krohe, A., 2001. Low-P/high-T pre-Alpine metamorphism and medium-P Alpine overprint of the Pelagonian Zone documented in high-alumina metapelites from the Vernon Massif, western Macedonia, northern Greece. Bull. Geol. Soc. Greece 34, 949–958.

Ohsaka, T., Izumi, F., Fujiki, Y., 1978. Raman spectrum of anatase, TiO_2. J. Raman. Spectrosc. 7, 321–324.

Okay, A.I., Satır, M., Siebel, W., 2006. Pre-Alpine Palaeozoic and Mesozoic orogenic events in the Eastern Mediterranean region. In: Gee, D., Stephenson, R. (Eds.), European Lithosphere Dynamics. Geol. Soc. Lond. Mem., vol. 32, pp. 389–405.

Okay, A.I., Satır, M., Tüysüz, O., Akyüz, S., Chen, F., 2001. The tectonics of the Strandja Massif: late-Variscan and mid-Mesozoic deformation and metamorphism in the northern Aegean. Int. J. Earth Sci. 90, 217–233.

Okrusch, M., Hock, R., Schüssler, U., Brummer, A., Baier, M., Theisinger, H., 2003. Intergrown niobian rutile phases with Sc- and W-rich ferrocolumbite: an electron-microprobe and Rietveld study. Am. Mineral. 88, 986–995.

Pober, E., Faupl, P., 1988. The chemistry of detrital chromian spinels and its implications for the geodynamic evolution of the Eastern Alps. Geol. Rundsch. 77, 641–670.

Porto, S.P.S., Fleury, P.A., Damen, T.C., 1967. Raman spectra of TiO_2, MgF_2, ZnF_2, FeF_2, and MnF_2. Phys. Rev. 154, 522–526.

Preston, J., Hartley, A., Mange-Rajetzky, M., Hole, M., May, G., Buck, S., 2002. The provenance of Triassic continental sandstones from the Beryl field, Northern North Sea: Mineralogical, geochemical, and sedimentological constraints. J. Sed. Res. 72, 18–29.

Robertson, A.H.F., Pickett, E.A., 2000. Palaeozoic–Early Tertiary Tethyan evolution of mélanges, rift and passive margin units in the Karaburun Peninsula (western Turkey) and Chios Island (Greece). In: Bozkurt, E., Winchester, J.A., Piper, J.D.A. (Eds.), Tectonics and Magmatism in Turkey and the Surrounding Area. Geol. Soc. Lond., Spec. Publ., vol. 173, pp. 43–82.

Rudnick, R.L., Barth, M., Horn, I., McDonough, W.F., 2000. Rutile-bearing refractory eclogites: missing link between continents and depleted mantle. Science 287, 278–281.

Sircombe, K.N., 1999. Tracing provenance through the isotope ages of littoral and sedimentary detrital zircon, eastern Australia. Sediment. Geol. 124, 47–67.

Spear, F.S., Wark, D.A., Cheney, J.T., Schumacher, J.C., Watson, B., 2006. Zr-in-rutile thermometry in blueschists from Sifnos, Greece. Contrib. Mineral. Petrol. 152, 375–385.

Spiegel, C., Siebel, W., Frisch, W., 2002. Sr and Nd isotope ratios of detrital epidote as provenance indicator and their significance for the reconstruction of the exhumation history of the Central Alps. Chem. Geol. 189, 231–250.

Stampfli, G.M., von Raumer, J., Borel, G.D., 2002. Palaeozoic evolution of pre-Variscan terranes: from Gondwana to the Variscan collision. In: Martínez-Catalán, J.R., Hatcher, R.D., Arenas, R., Díaz García, F. (Eds.), Variscan–Appalachian Dynamics: The Building of the Late Paleozoic Basement. Geol. Soc. Am., Spec. Pap., vol. 364, pp. 263–280.

Stampfli, G.M., Vavassis, I., De Bono, A., Rosselet, F., Matti, B., Bellini, M., 2003. Remnants of the Paleotethys oceanic suture-zone in the western Tethyan area. In: Cassinis, G., Decandia, F.A. (Eds.), Stratigraphic and Structural Evolution on the Late Carboniferous to Triassic Continental and Marine Successions in Tuscany (Italy): Regional Reports and General Correlation. Boll. Soc. Geol. Ital., vol. spec. 2, pp. 1–23.

Stendal, H., Toteu, S.F., Frei, R., Penaye, J., Njel, U.O., Bassahak, J., Nni, J., Kankeu, B., Ngako, V., Hell, J.V., 2006. Derivation of detrital rutile in the Yaoundé region from the Neoproterozoic Pan-African belt in southern Cameroon (Central Africa). J. Afr. Earth Sci. 44, 443–458.

Tompsett, G.A., Bowmaker, G.A., Cooney, R.P., Metson, J.B., Rodgers, K.A., Seakins, J.M., 1995. The Raman spectrum of brookite, TiO_2 (*Pbca*, $Z=8$). J. Raman Spectrosc. 26, 57–62.

Topuz, G., Altherr, R., Kalt, A., Satır, M., Werner, O., Schwarz, W.H., 2004. Aluminous granulites from the Pulur Complex, NE Turkey: a case of partial melting, efficient melt extraction and crystallization. Lithos 72, 183–207.

Triebold, S., von Eynatten, H., Zack, T., 2005. Trace elements in detrital rutile as provenance indicator: A case study from the Erzgebirge, Germany. In: Haas, H., Ramseyer, K., Schlunegger, F. (Eds.), Sediment 2005, Abstracts. Schriftenr. Dt. Ges. Geowiss., vol. 38, pp. 144–145.

Triebold, S., von Eynatten, H., Luvizotto, G.L., Zack, T., 2007. Deducing source rock lithology from detrital rutile geochemistry: an example from the Erzgebirge, Germany. Chem. Geol. doi:10.1016/j.chemgeo.2007.06.033.

Turpaud, P., Reischmann, T., 2005. Relationships between crustal blocks and UHP relics, an example from Northern Greece. Geophys. Res. Abstr. 8, 04353.

Uher, P., Černý, P., Chapman, R., Határ, J., Miko, O., 1998. Evolution of Nb, Ta-oxide minerals in the Prašivá granitic pegmatites, Slovakia. I. Primary Fe, Ti-rich assemblage. Can. Mineral. 36, 525–534.

Vavassis, I., De Bono, A., Stampfli, G.M., Giorgis, D., Valloton, A., Amelin, Y., 2000. U–Pb and Ar–Ar geochronological data from the Pelagonian basement in Evia (Greece): geodynamic implications for the evolution of Paleotethys. Schweiz. Miner. Petrogr. Mitt. 80, 21–43.

von Eynatten, H., Gaupp, R., 1999. Provenance of Cretaceous synorogenic sandstones from the Eastern Alps: constraints from framework petrography, heavy mineral analysis, and mineral chemistry. Sediment. Geol. 124, 81–111.

von Eynatten, H., Tolosana-Delgado, R., Triebold, S., Zack, T., 2005. Interactions between grain size and composition of sediments: two examples. Proceed. 2nd CoDaWork, 19–21 October 2005, Girona, Spain.

Watson, E.B., Wark, D.A., Thomas, J.B., 2006. Crystallization thermometers for zircon and rutile. Contrib. Mineral. Petrol. 151, 413–433.

Zack, T., Luvizotto, G.L., 2006. Application of rutile thermometry to eclogites. Mineral. Petrol. 88, 69–85.

Zack, T., Moraes, R., Kronz, A., 2004a. Temperature dependence of Zr in rutile: empirical calibration of a rutile thermometer. Contrib. Mineral. Petrol. 148, 471–488.

Zack, T., von Eynatten, H., Kronz, A., 2004b. Rutile geochemistry and its potential use in quantitative provenance studies. Sediment. Geol. 171, 37–58.

Zack, T., Kronz, A., Foley, S.F., Rivers, T., 2002. Trace element abundances in rutiles from eclogites and associated garnet mica schists. Chem. Geol. 184, 97–122.

Zanchi, A., Garzanti, E., Larghi, C., Angiolini, L., Gaetani, M., 2003. The Variscan orogeny in Chios (Greece): Carboniferous accretion along a Palaeotethyan active margin. Terra Nova 15, 213–223.